Nanobeads highly loaded with superparamagnetic nanoparticles prepared by emulsification and seeded-emulsion polymerization

Paquet, Chantal; Page, Lilianne; Kell, Arnold; Simard, Benoit

Publisher's version / Version de l'éditeur:
https://doi.org/10.1021/la903815t
Langmuir, 26, 8, pp. 5388-5396, 2010-04-20

Langmuir
Article
pubs.acs.org/Langmuir
Published 2009 by the American Chemical Society

Nanobeads Highly Loaded with Superparamagnetic Nanoparticles Prepared by Emulsification and Seeded-Emulsion Polymerization

Chantal Paquet,* Lilianne Pagé, Arnold Kell, and Benoit Simard*

Steacie Institute for Molecular Sciences, National Research Council, 100 Sussex Drive, Ottawa, Ontario, Canada, K1A 0R6

Received October 8, 2009. Revised Manuscript Received November 20, 2009

Functional superparamagnetic colloids possessing high saturation magnetization are prepared by emulsification of superparamagnetic nanoparticles (SPM NPs) and heterogeneous polymerization. The colloids consist of a core of densely packed NPs encapsulated within a thin polymer shell. The cores are made by emulsifying SPM NPs and toluene into an aqueous surfactant solution, and subsequently condensing the emulsion droplets by removal of the solvent generating clusters of SPM NPs. By tuning the emulsification condition, this approach allows for control over the size of the clusters from approximately 40 to 200 nm. The polymer shells encapsulating the clusters are made by using seeded-emulsion polymerization concepts. Control over the thickness of the shell and the incorporation of functional groups to the colloid is achieved. Characterization by thermogravimetric analysis (TGA) and magnetometry shows that these colloids have 66 wt % of magnetic material and saturation magnetization of 47 emu/g, confirming that this route generates colloids with a high loading of SPM NPs and high saturation magnetizations.

1. Introduction

Colloids with superparamagnetic functionality are commonly used as substrates for separating and purifying biomolecules and cells from complex mixtures.[1−3] Micrometer and submicrometer colloids are better suited over nanometer colloids for such conventional uses of magnetic beads, as their larger volume can accommodate a greater number of superparamagnetic nanoparticles (SPM NPs), imparting them with higher magnetophoretic mobilities.[4] However, current interest in micro-total-analysis systems (μ-TASs) using microfluidic platforms[5] and in vivo applications (e.g., magnetic resonance imaging (MRI), drug delivery vehicles, hyperthermia therapeutic)[6−8] has shifted the demand for nanometer-sized superparamagnetic colloids (i.e., ∼100 nm). Because of their small volumes, these colloids hold a fewer number of SPM NPs, causing them to respond undesirably slow to magnetic fields gradients. Therefore, designing magnetic meso- and nanobeads that minimize the volume of the nonmagnetic matrix material and maximize the volume of SPM NPs is of prime importance. Here we describe a method of preparing magnetic nanobeads based on combining emulsification and seeded-emulsion polymerization concepts. This approach produces particles with diameters ranging from approximately 40 to 200 nm with size control and the presence of functional groups for incorporating surface ligands. Most important, because of the high loading of magnetic material, these nanobeads possess a high mass magnetization and thus maintain a rapid response to magnetic field gradients.

Many reports describe methods of incorporating inorganic nanoparticles into colloids. For instance, composite colloids can be prepared by swelling polymer beads and subsequently diffusing nanoparticles into their interior.[9−12] Also, hybrid colloids have been prepared by in situ synthesis of nanoparticles in the interior of premade colloids.[13−15] Alternatively, colloids prepared by heteropolymerization in the presence of nanoparticles have produced composite colloids.[16−19] These routes generally generate colloids with micro- and submicrometer diameters and often can not be adapted to make smaller meso- or nanosized colloids. Furthermore, the modest loadings of nanoparticles per colloid that these routes yield render the nanobeads with impractically low magnetophoretic mobilities.

Recent reports have acknowledged this shortcoming and have offered routes to preparing aggregates of nanoparticles. These structures are clusters of nanoparticles with little or no matrix materials, and thus have a high concentration of magnetic material. Approaches to preparing such clusters have included the aggregation and crystallization of SPM NPs using solvophobic interactions,[20] by solvothermal reduction reactions between

*To whom correspondence should be addressed. E-mail: chantal.paquet@nrc.ca or benoit.simard@nrc.ca. Phone: 613-990-0977. Fax: 613-991-2648.

(1) Ugelstad, J.; Stenstad, P.; Kilaas, L.; Prestvik, W. S.; Herje, R.; Berge, A.; Hornes, E. *Blood Purification* **1993**, *11*, 349–369.
(2) Horak, D.; Babic, M.; Mackova, H.; Benes, M. J. *J. Sep. Sci.* **2007**, *30*, 1751–1772.
(3) McCloskey, K. E.; Chalmers, J. J.; Zborowski, M. *Anal. Chem.* **2003**, *75*, 6868–6874.
(4) Gijs, M. A. M. *Microfluidics Nanofluidics* **2004**, *1*, 22–40.
(5) Lai, J. J.; Nelson, K. E.; Nash, M. A.; Hoffman, A. S.; Yager, P.; Stayton, P. S. *Lab Chip* **2009**, *9*, 1997–2002.
(6) Corr, S. A.; Byrne, S. J.; Tekoriute, R.; Meledandri, C. J.; Brougham, D. F.; Lynch, M.; Kerskens, C.; L, O. D.; Gun'ko, Y. K. *J. Am. Chem. Soc.* **2008**, *130*, 4214–4215.
(7) Larsen, B. A.; Haag, M. A.; Serkova, N. J.; Shroyer, K. R.; Stoldt, C. R. *Nanotechnology* **2008**, *19*, 8–14.
(8) Picard, F. J.; Bergeron, M. G. *Drug Discovery Today* **2002**, *7*, 1092–1101.
(9) Bradley, M.; Bruno, N.; Vincent, B. *Langmuir* **2005**, *21*, 2750–2753.
(10) Han, M.; Gao, X.; Su, J. Z.; Nie, S. *Nat. Biotechnol.* **2001**, *19*, 631–635.
(11) Gorelikov, I.; Field, L. M.; Kumacheva, E. *J. Am. Chem. Soc.* **2004**, *126*, 15938–15939.
(12) Kuang, M.; Wang, D.; Bao, H.; Gao, M.; Möhwald, H.; Jiang, M. *Adv. Mater.* **2005**, *17*, 267–270.
(13) Zhang, J.; Xu, S.; Kumacheva, E. *J. Am. Chem. Soc.* **2004**, *126*, 7908–7914.
(14) Cen, L.; Neoh, K. G.; Kang, E. T. *Adv. Mater.* **2005**, *17*, 1656–1661.
(15) Dokoutchaev, A.; Thomas James, J.; Koene, S. C.; Pathak, S.; Surya Prakash, G. K.; Thompson, M. E. *Chem. Mater.* **1999**, *11*, 2389–2399.
(16) Ramírez, L. P.; Landfester, K. *Macromol. Chem. Phys.* **2003**, *204*, 22–31.
(17) Joumaa, N.; Lansalot, M.; Théretz, A.; Elaissari, A.; Sukhanova, A.; Artemyev, M.; Nabiev, I.; Cohen, J. H. M. *Langmuir* **2006**, *22*, 1810–1816.
(18) Ramírez, L. P.; Landfester, K. *Macromol. Chem. Phys.* **2003**, *204*, 22–31.
(19) Erdem, B.; Sudol, E. D.; Dimonie, V. L.; El-Aasser, M. S. *J. Polym. Sci., Part A* **2000**, *38*, 4431–4440.
(20) Zhuang, J. Q.; Wu, H. M.; Yang, Y. G.; Cao, Y. C. *Angew. Chem., Int. Ed.* **2008**, *47*, 2208–2212.

$FeCl_3$ and ethylene glycol,[21] using a microemulsion approach,[22] and, by growth through competitive stabilizer desorption.[23] Due to the high content of magnetic material, these nanoaggregates of SPM NPs possess large mass magnetizations and thus hold promise as probes, carriers, and substrates in applications that require rapid magnetic responses.[24] However, many of these routes produce structures that lack the functional surface groups that are required for anchoring molecular recognition agents.

In this report, we describe a route to preparing functional superparamagnetic nanobeads with high saturation magnetization. More specifically, the structures of these colloids consist of a core of densely packed SPM NPs encapsulated in a thin polymer shell. The cores of SPM NPs are made by first emulsifying SPM NPs dispersed in organic solvent into an aqueous phase. The organic solvent is subsequently removed generating clusters of SPM NPs. These clusters are then encapsulated with a polymer shell using seeded-emulsion polymerization concepts.

This report is divided into three sections. In the first section, the approach of preparing superparamagnetic nanobeads is introduced. The second section examines the formation of clusters of SPM NPs, including (i) the role of the emulsification conditions, (ii) the effect of the composition of the emulsion, and (iii) an overview of the parameters that govern the polydispersity of clusters. In the third part of the paper, we describe how seeded-emulsion polymerization is used to encapsulate clusters to form functional nanobeads. The properties of the nanobeads, such as the magnetic properties and the surface functionality, are characterized. We show that these nanobeads possess features desirable for bioseparation applications such as high saturation magnetizations, control over the size of the colloid, and high surface functionality.

2. Experimental Section

Materials. ACS-grade sodium dodecyl sulfate (SDS; 99+%), glycidyl methacrylate (GMA), ethyl glycol dimethacrylate (EGDMA), and potassium persulfate were purchased from Sigma-Aldrich. Superparamagnetic iron oxide nanoparticles (SPM NPs) coated with fatty acids were purchased from Ferrotec. The Ferrotec SPM NPs were analyzed by transmission electron microscopy (TEM) image analysis and found to have a diameter of 9.1 ± 2.7 nm. Water filtered through a Millipore filtration system was used for all syntheses and experiments. Lucifer yellow cadavarine was purchased from Invitrogen.

Preparation of Clusters. The SPM NPs were dispersed in toluene at a concentration of 0.05 g/mL unless otherwise stated. Using a Branson Sonifier 250 (maximum output power of 200 W) with a Branson tapered microtip (3 mm), the SPM NP dispersions were sheared in an aqueous SDS solution with a droplet to a continuous phase volume ratio of 0.09 for 120 s with an output power of 80 W and a duty cycle of 50% unless otherwise noted. The emulsions were left to ripen for a given time and subsequently heated at 90 °C for 2 h. Water was added intermittently to maintain a constant volume.

Preparation of Nanobeads. Excess surfactant in the cluster dispersion was reduced by dialysis or centrifugation/redispersion. Clusters (0.2 g) were diluted to 100 mL of water, and the SDS concentration was adjusted to 1−5 mM. The cluster dispersions were placed in a three-neck round-bottom flask with a temperature probe and condenser attached to two of the necks. The clusters were stirred and heated to 80 °C under a flow of nitrogen. Once the temperature stabilized, 0.075 mL of a 10% vol/vol mixture of EGDMA/GMA was added, and, immediately following, 1 mg of potassium persulphate diluted in 0.5 mL of water was injected. The monomers were left to polymerize for 3 h. The polymer-coated clusters were purified by centrifugation and redispersion.

Coupling of Lucifer Yellow to Nanobeads. A solution of 0.50 mg of Lucifer yellow cadaverine in 10 mL of phosphate buffer was prepared. A 500 μL aliquot of this solution was mixed with 20 μL of a 3.9 mg/mL dispersion of nanobeads. The sample was stirred overnight and purified by magnetically separating and redispersing the beads three times. Photoluminescence of the nanobeads was acquired by diluting the beads in 1 mL of phosphate buffer. The concentration of Lucifer yellow cadaverine on the beads was determined by comparing the photoluminescence against a calibration curve of known concentrations of lucifer yellow cadavarine in phosphate buffer.

Instrumentation. Thermogravimetric analysis (TGA) was performed on a Netzsch TG/MS/FTIR system (Netzsch TG 209 F1 Iris coupled to an Aëolos QMS403C mass spectrometer and a Bruker Tensor 27 Fourier Transform Infrared spectrometer via a TGA A588 TGA-IR module) under a flow of compressed air to ensure complete oxidation, while the balance was protected under a flow of ultrahigh pure argon (99.9993%). Light extinction of the emulsions was measured at $\lambda = 600$ nm on a Cary STD spectrophotometer from Varian using a cuvette with a path length of 1 mm. Hydrodynamic diameters were determined by dynamic light scattering (DLS) using a Malvern Zetasizer 3000HS. TEM imaging was performed on an Hitachi HD-2000. Cluster diameters and size distributions were determined by analyzing TEM images using ImageTool software. The viscosities of fluids were measured using a Brookfield RV-DV-III ultra Rheometer, with a UL adapter for low viscosity fluids. An Oakton instrument, model EC Testr low, was used to measure the conductance of the emulsions. An IKA T10 basic Ultra-Turrax was used to compare sheared emulsion. A Fluorolog by Yvon-Jobin was used to acquire photoluminesce spectra. Spectra ranging from 440 to 700 nm using an excitation wavelength of 425 nm and slits of 4.0 nm were used to acquire spectra of Lucifer yellow cadaverine. The magnetic susceptibility measurements were obtained with the use of a Quantum Design SQUID magnetometer MPMS-XL. This magnetometer works between 1.8 and 400 K for direct current (dc) applied fields ranging from −7 to 7 T. Measurements were performed on nanoparticles of 10.5 mg of Ferrotec, 10.6 mg of nanobeads, and 9.9 mg of clusters. The magnetic data were corrected for the sample holder and the diamagnetic contributions.

3. Results and Discussion

3.1. Overview of the Nanobeads. As shown in Scheme 1, the process of forming nanobeads can be divided into three steps. (i) SPM NPs dispersed in toluene are emulsified into an aqueous solution of SDS, producing "oil" droplets (i.e., SPM NPs in organic solvent) of a few micrometers. At this stage, the emulsion can be left to ripen. (ii) Next, the droplets are condensed into clusters of SPM NPs by evaporating the toluene within the emulsion droplet. (iii) The clusters of SPM NPs are then encapsulated with a polymer shell using emulsion polymerization concepts.

The TEM images found in Figure 1a show the densely packed structure of clusters, while Figure 1b,c illustrates the structure of the polymer-encapsulated clusters. As will be discussed later, the TGA of the individual nanoparticles and the clusters as a whole show that these clusters are made up of 1% surfactant and 99% of the NPs. Therefore, the clusters are densely packed NPs stabilized by the surfactant present at the interface of the colloid. We speculate that the SDS molecules interdigitate in the layer of

(21) Ge, J. P.; Hu, Y. X.; Biasini, M.; Beyermann, W. P.; Yin, Y. D. *Angew. Chem., Int. Ed.* **2007**, *46*, 4342–4345.
(22) Bai, F.; Wang, D. S.; Huo, Z. Y.; Chen, W.; Liu, L. P.; Liang, X.; Chen, C.; Wang, X.; Peng, Q.; Li, Y. D. *Angew. Chem., Int. Ed.* **2007**, *46*, 6650–6653.
(23) Stolarczyk, J. K.; Ghosh, S.; Brougham, D. F. *Angew. Chem., Int. Ed.* **2008**, *48*, 175–178.
(24) Xu, H.; Cui, L. L.; Tong, N. H.; Gu, H. C. *J. Am. Chem. Soc.* **2006**, *128*, 15582–15583.

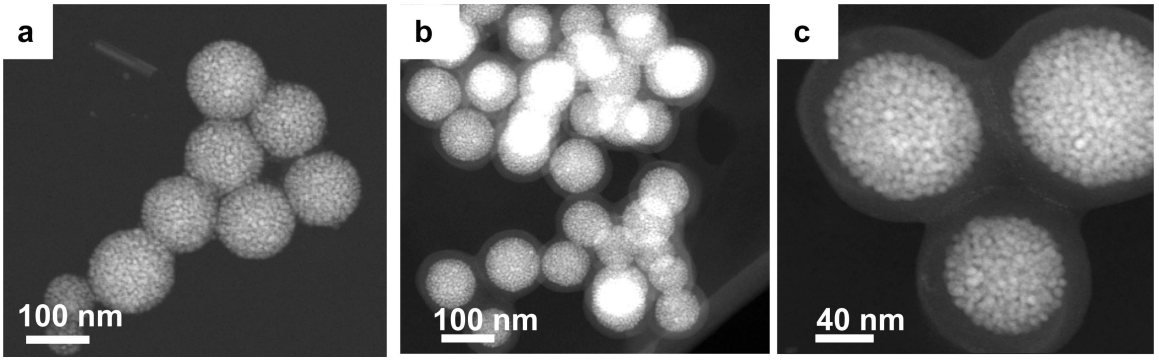

Figure 1. TEM image of (a) clusters of SPM NPs and (b,c) magnetic nanobeads made from polymer-encapsulated clusters.

Scheme 1. Process of Nanobead Formation[a]

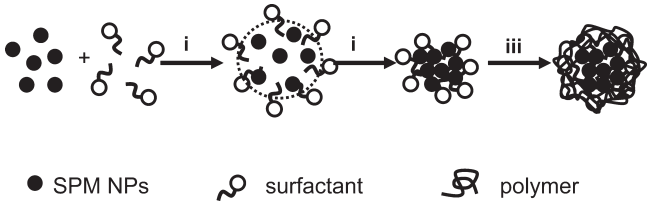

[a] SPM NPs dispersed in organic solvent are ultrasonicated with an aqueous solution of surfactant and left to ripen (i). Next the emulsion droplets are transformed into cluster by evaporating the solvent within the droplet (ii). The clusters are encapsulated in a thin polymer shell using seeded-emulsion polymerization concepts (iii).

ligands (fatty acids) surrounding the SPM NPs.[25,26] The hydrophobic nature of the nanoparticles keeps the clusters aggregated and prevents them from breaking up in the aqueous environment, while the presence of the surfactant at the surface of the clusters maintains stability against coalescence.

3.2. Preparation of Clusters. We set out to understand each step in the preparation of the clusters in order to establish which parameters control their size and size distribution. To this end, emulsions were prepared under varying conditions and condensed into clusters, and the size and size distribution of the clusters were measured by DLS and TEM. Knowledge of the size of the droplet prior to condensing them into clusters can provide insight into the mechanism of the emulsification and cluster formation. Therefore, we verified that the droplets went unchanged during the condensing step (i.e., absence of fission or fusion of the droplets during the condensing step), in order to use the size of the clusters as a measure of the droplet size. To verify this idea, emulsion droplets were condensed at different rates by using different evaporation temperatures. We found that the diameters of the cluster differed by less than 4 nm when prepared at 21 and 95 °C (corresponding to an evaporation time of approximately ~12 and 1 h, respectively). In addition, no significant changes in the structure, size, or size distributions were observed in the TEM images of these samples. On the basis of these results, we conclude that no significant changes occur to the droplet when evaporating the solvent, and, accordingly, the clusters are made up of the same number of SPM NPs as the droplet before solvent evaporation.

3.2.1. Ultrasonication to a Steady State. The emulsification of an oil phase into an aqueous phase produces droplets that are kinetically stabilized, and, as a result, the droplet size and size distribution depend on the intensity and duration of the shearing unless a steady-state of droplet fission/fusion is reached. Therefore, the conditions that generate emulsions at a steady-state of droplet fusion and fission were determined. Figure 2 shows that, for emulsions prepared with two different concentrations of SDS, C, and sonicated for 180 s, the size of the clusters decreases when the power level of the ultrasonicator increases. When the power level was kept constant and the duration of ultrasonication was varied, the diameter of the clusters changed marginally after 90 s. Therefore, for this study, emulsions were prepared by sonicating at an output power of 80 W level for 180 s.

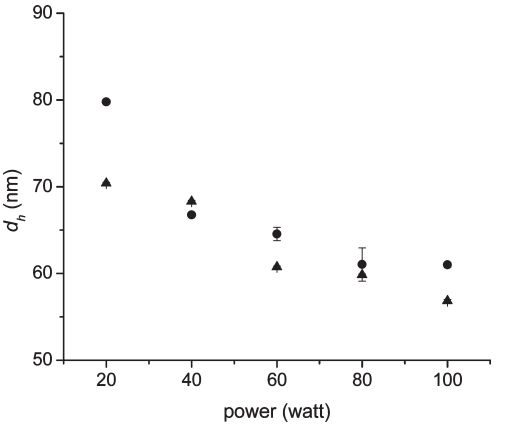

Figure 2. Dependence of the diameter on the sonifier output power for emulsions prepared with $C = 5$ mM (●) and 50 mM (▲).

3.2.2. The Role of Ripening the Emulsions. Postsonication, kinetically stabilized emulsion can undergo a ripening process either via the droplets coalescing or by Ostwald ripening, where solvent diffuses from smaller and more unstable droplets to larger droplets. Both of these processes lead to an increase in the average size of the droplet. Ostwald ripening can be suppressed by adding a highly water-insoluble species into the oil phase (such systems are referred to as mini-emulsions). Typically, the hydrophobes must be present in high enough molar concentrations with respect to the oil phase for the hydrophobe to allow an osmotic pressure to build up in the droplet, suppressing diffusion and providing stability against this ripening mechanism. An analogy can be made between the emulsions studied here and mini-emulsions prepared for latex particles, which typically use hexadecane as a hydrophobe to stabilize monomer droplets.[27,28] In the present system, toluene is analogous to a monomer since it is slightly

(25) Wu, H.; Zhu, H.; Zhuang, J.; Yang, S.; Liu, C.; Cao, Y. C. *Angew. Chem., Int. Ed.* **2008**, *47*, 3730–3734.
(26) Fan, H. Y.; Leve, E.; Gabaldon, J.; Wright, A.; Haddad, R. E.; Brinker, C. J. *Adv. Mater.* **2005**, *17*, 2587–2590.
(27) Landfester, K.; Bechthold, N.; Tiarks, F.; Antonietti, M. *Macromolecules* **1999**, *32*, 5222–5228.
(28) Anderson, C. D.; Sudol, E. D.; El-Aasser, M. S. *Macromolecules* **2002**, *35*, 574–576.

water-soluble, and the nanoparticles can act as a hydrophobe because of their low water solubility.

The effect of maturing the emulsion was initially examined by measuring the size of the clusters as a function of ripening time (i.e., the time between sonication and condensation). When clusters were prepared and left to ripen for various durations ranging from 0 to 96 h, no changes in the size of the clusters were observed. This result implies that coalescence of the droplet postsonication does not occur. Despite this result, we observed decreases in the opacity of the emulsions with time. Therefore, to monitor the changes in the emulsions, the light extinction and conductance of the emulsion were monitored. Light extinction (E) gives a measure of scattering by the emulsion, which in this case is determined by the refractive index contrast between the two phases, the number of particles, and most dominantly by the diameter of the droplets ($E \approx r^6$ where r is the radius of the particle).[29,30] Therefore, light extinction can give a measure of changes in the average particle size as time evolves. Conversely, the conductance of the emulsion is a measure of the partitioning of SDS molecules between the oil−water interface and the aqueous phase. For instance, when the area of the oil−water interface increases, the equilibrium of SDS shifts toward stabilizing the interface, thereby decreasing the concentration of aqueous SDS and lowering the conductance of the emulsion. In this manner, conductance provides a measure of total surface area of the oil droplets.[31] Figure 3a,b shows the changes in the light extinction and conductance of emulsions (C = 10 mM and 50 mM) ripened for 200 h and subsequently condensed into clusters. The plots show that, during the ripening stage, the emulsions undergo a rapid decrease followed by a slower decrease in the conductance and light extinction. Once the emulsions are left to condense from droplet to cluster (indicated by the dotted lines), a dramatic increase in the conductance is observed along with a slight decrease in light extinction. The effect is more pronounced for emulsion prepared with higher concentrations of SDS. A possible scenario, described schematically in Figure 4, which can explain these observations, is as follows. Once sonication is complete, an emulsion is formed of primary droplets containing toluene and a certain number of SPM NPs. For the concentration of SPM NPs used here, the molar ratio of SPM NPs to toluene is approximately 1:300 000, a concentration much lower than the 1:250 molar ratio required to suppress Ostwald ripening.[27] Thus, Ostwald ripening of toluene occurs, toluene diffuses out of the droplet and, with the excess surfactant in the aqueous phase, forms solvent-swollen micelles. These events lead to a decrease in the average diameter of the droplets, producing a drop in the light extinction. The increase in the total surface area of the oil−water interface generated from newly formed solvent−swollen micelles causes the initial drop in conductance. Once toluene is left to evaporate (water is added to keep the volume constant), the primary droplets transform into clusters, while the solvent-swollen micelles form a mixture of empty micelles and free SDS. These transformations create a decrease in the average diameter of particles and the oil−water surface area, which is measured as a further decrease in light extinction and a dramatic increase in the conductance. It is important to note that, throughout this ripening process, the primary droplets maintain a constant number of SPM NPs since the nanoparticles do not have high enough water solubility to diffuse from the primary droplet.

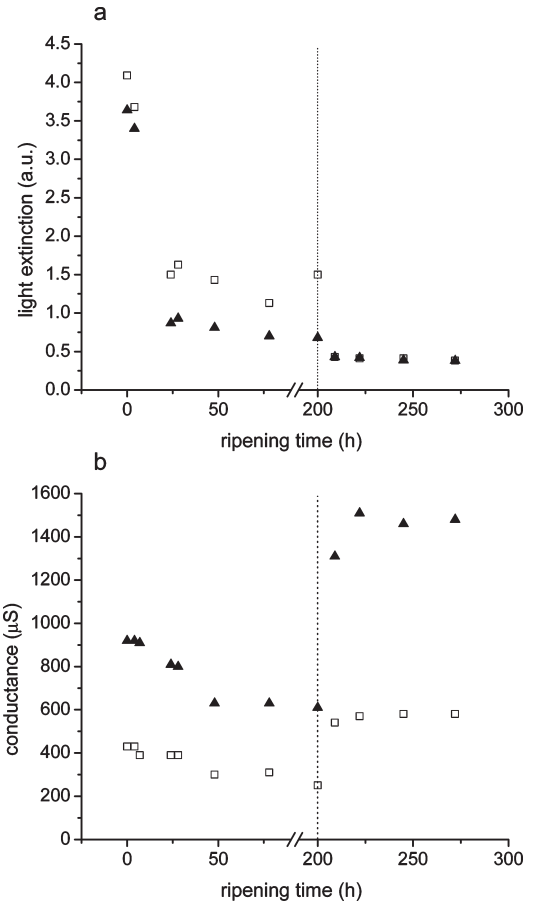

Figure 3. The dependence of (a) light extinction and (b) conductance of emulsions as a function of ripening time for emulsions prepared with C = 10 mM (□) and 50 mM (▲). The dotted lines indicate the time at which evaporation was started.

This explanation is consistent with the observation that the size of the clusters does not change regardless of the duration of ripening. On the basis of this description of the processes that take place after sonication, ripening the emulsion postsonication does not affect the size and size distribution of the clusters.

3.2.3. The Role of the Composition of the Emulsion. During emulsification, shear forces work against the interfacial tension (σ) of a droplet to elongate and break the droplet into smaller ones. Coalescence of these droplets is prevented by the repulsive forces provided by the surfactant found at the interface. The composition of the emulsions plays a key role in the emulsification process, as it determines the balance between the interfacial tension and viscous shear stress. On the basis of a simple model of an isolated droplet rupturing into two daughter droplets of approximately the same size (binary breakup) by a viscous shear force, the average radius of the daughter droplets has been proposed to follow

$$r \approx \frac{\lambda\sigma}{\eta_c \dot{\gamma}} \qquad (1)$$

for $\lambda \sim 1$, where λ is the ratio of the droplet to continuous phase viscosities ($\lambda = \eta_d/\eta_c$) and $\eta_c\dot{\gamma}$, is the viscous shear force (η_c is the viscosity of the continuous phase ,and $\dot{\gamma}$ is the shear rate).[32,33]

(29) Farinato, R. S., Rowell, R. L. In *Encyclopedia of Emulsion Technology*; Becher, P., Eds.; M. Dekker: New York, 1983; Vol. *1*, p 439.
(30) Baloch, M. K.; Hameed, G. *J. Colloid Interface Sci.* **2005**, *285*, 804–813.
(31) Landfester, K.; Bechthold, N.; Förster, S.; Antonietti, M. *Macromol. Rapid Commun.* **1999**, *20*, 81–84.
(32) Rallison, J. M. *Annu. Rev. Fluid Mech.* **1984**, *16*, 45–66.
(33) Torza, S.; Cox, R. G.; Mason, S. G. *J. Colloid Interface Sci.* **1972**, *38*, 395–411.

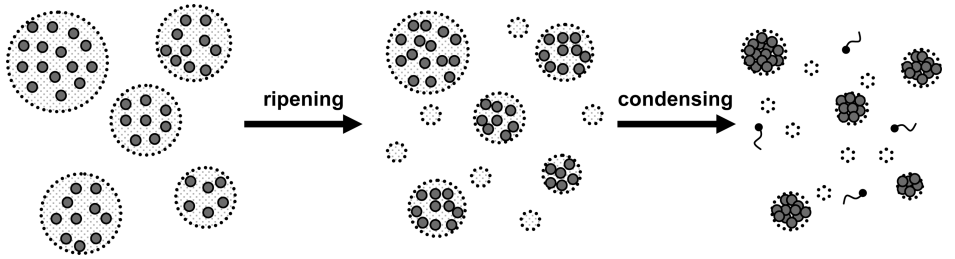

Figure 4. Emulsions formed from ultrasonication left to ripening. During this time, solvent-swollen micelles are formed. Once the solvent is left to evaporate, clusters and SDS micelles form, reducing the total oil−water surface area.

Although the above relationship has successfully described rupturing of droplets under certain conditions, the relationship has significant limitations. First, surfactant solutions making up the continuous phase as well as concentrated emulsions can exhibit viscoelasticity, yielding under low shear deformation but flowing for larger shear deformations.[34−37] Under these circumstances, the viscosities at high shear rates have in some instances explained the observed droplet sizes. Second, when λ is larger or much smaller than unity, larger shear deformations are required to break up the droplets.[33] Third, this model does not account for droplets formed by other types of rupturing mechanisms. For instance, tip streaming occurs when a droplet under shear rotates, forming pointed ends that are pinched off as much smaller droplets.[38] Break-up under capillary instability on the other hand occurs when highly elongated droplets that develop under certain shearing conditions form undulated threads due to heterogeneities in the surface tensions, which in turn break up into many smaller droplets.

Although this model has several shortcomings, it is nonetheless a useful guide in understanding very generally how the composition of the emulsion determines droplet size. The purpose of this section is to describe how the concentration of SDS, C, the concentration of SPM NPs dispersed in toluene, f, and the volume ratio of the droplet to continuous phase, ϕ, govern the size of clusters (or droplets), within the framework of droplets rupturing by viscous shear forces. As previously discussed, we assume that SPM NPs do not exchange from droplet to droplet postemulsification. Therefore, we interchange the terms droplets and clusters, referring to the size of the droplets as they were immediately following emulsification. Although our experiments do not cover all combinations and ranges of C, f, and, ϕ, the study does identify trends, and we are able to elucidate how these parameters dictate the size and size distribution of the clusters.

Emulsions were prepared with C varying from 1 to 100 mM and for fixed values of $f = 0.05$ g/mL and $\phi = 0.09$. Below 3 mM, stable emulsion could not be obtained. As shown in Figure 5b, for concentrations between 3 and 15 mM, the diameters of the clusters decrease with increasing concentration of surfactant. This initial drop in cluster size (or droplet) parallels previous studies, and is in agreement with eq 1, which predicts a drop in the droplet size with decreasing interfacial tension resulting from adding surfactant.[27,28] In contrast to previous studies, which report a leveling off of droplet size at high surfactant concentrations, we observed an increase in the size of the clusters for $C > 15$ mM (Figure 5a).[28] Although it is true that concentrated SDS solutions undergo shear thinning (see Supporting Information), shear thinning was ruled out as a possible explanation, as the viscosities at high shear rates change marginally with increasing concentration of SDS. It is, however, interesting to note that the transition in size occurs slightly above the critical micelle concentration of SDS (~8 mM).[39,40] We propose two possible scenarios to explain this observation. As has been observed and explained elsewhere, SDS molecules align under shear forces. Under these conditions, the viscous flow of the continuous phase can fracture, causing a decrease in the effective shear force.[36,41] This decrease in the

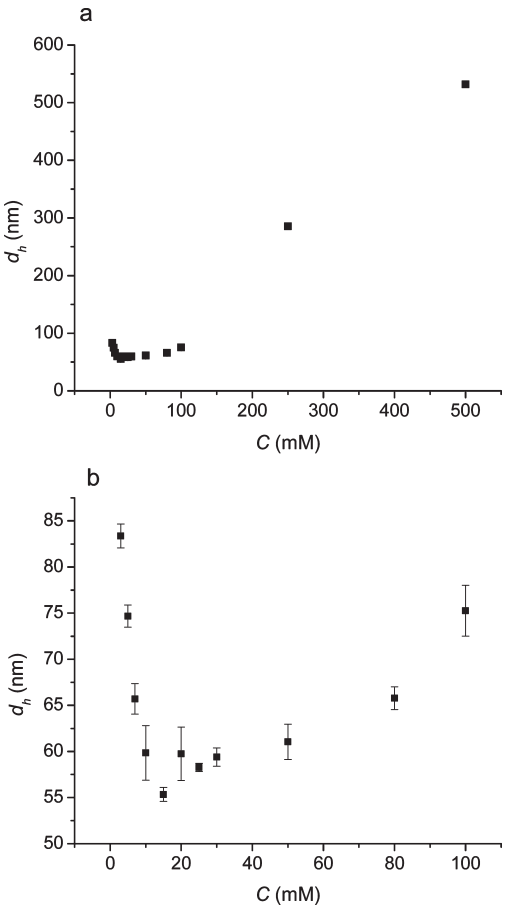

Figure 5. The effect of the concentration of SDS for (a) concentrations up to 500 mM and (b) concentrations below 100 mM on the diameter of the clusters prepared with $f = 5$ g/mL and $\phi = 0.09$.

(34) Mason, T. G.; Bibette, J. *Phys. Rev. Lett.* **1996**, *77*, 3481–3484.
(35) Mason, T. G.; Bibette, J. *Langmuir* **1997**, *13*, 4600–4613.
(36) Mason, T. G.; Bibette, J.; Weitz, D. A. *J. Colloid Interface Sci.* **1996**, *179*, 439–448.
(37) Jansen, K. M. B.; Agterof, W. G. M.; Mellema, J. *J. Rheol.* **2001**, *45*, 227–236.
(38) De Bruijn, R. A. *Chem. Eng. Sci.* **1993**, *48*, 277–284.
(39) On the basis of the conductivity of SDS solutions, a critical micelle concentration of 7.7 mM was determined. On the basis of a previous study of changes in the critical micelle concentration of SDS in macroemulsion, we expect the critical micelle concentration to increase to ~8−9 mM.
(40) Chang, H.-C.; Lin, Y.-Y.; Chern, C.-S.; Lin, S.,Y. *Langmuir* **1998**, *14*, 6632–6638.
(41) Diat, O.; Roux, D.; Nallet, F. *Phys. Rev. E* **1995**, *51*, 3296–3299.

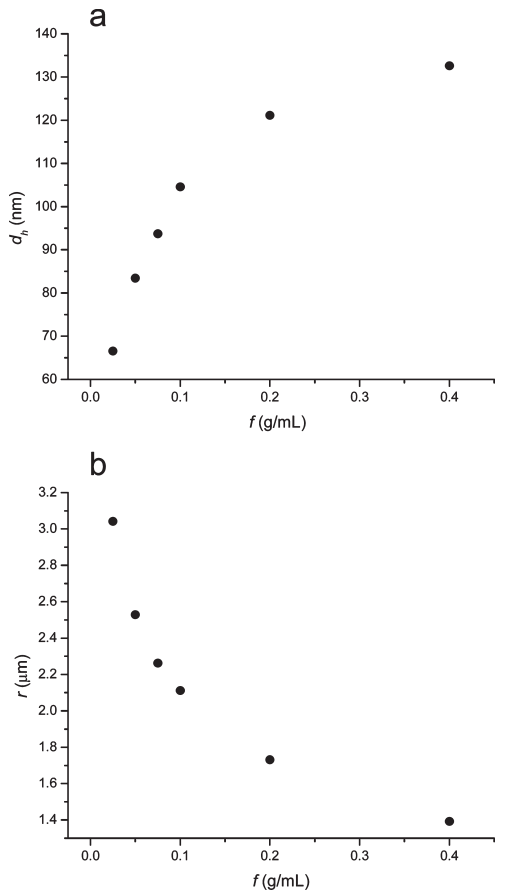

Figure 6. The effect the concentration of SPM NPs on (a) the diameter of the clusters and (b) the radius of the droplets (C = 50 mM and ϕ = 0.09).

effective shear force in turn increases the average diameter of the droplets. Thus, as the SDS concentration increases and ordered structure of SDS begin to form, fractured flow occurs, lowering the effective shear forces and decreasing the average droplet size. An alternative explanation takes into account depletion forces, which occur between droplets in the presence of micelle. Micelles, which are driven to increase their free volume in solution, create an attractive force between larger droplets (i.e., depletion forces). As the concentration of SDS increases above the critical micelle concentration, this attractive force between droplets develops, inducing coalescence of the droplets and increasing the average diameter of the droplets.

The concentration of SPM NPs in toluene, f, used to prepared clusters was expected to play an important role in determining the size of the clusters. As shown earlier, because SPM NPs do not diffuse from droplet to droplet postsonication, varying the concentration of SPM NPs in the droplet phase can provide a convenient means to control cluster size. The sizes of clusters prepared from emulsion with f ranging from 0.025 to 0.4 g/mL are found in Figure 6a (for C = 50 mM and ϕ = 0.09). The results demonstrate that the diameter of the clusters increase monotonically with increasing f. To gain more insight into these results, the sizes of the droplet that formed these clusters were calculated based on the size of the clusters and the value of f. As shown in Figure 6b, the droplet radii decrease with increasing f and appear to level off at high values of f. We believe the decrease in droplet size with increasing concentration of SPM NPs can be explained by considering the viscosity ratio of the droplet to continuous phase ($\lambda = \eta_d/\eta_c$). The viscosities of the droplet phase for f = 0.2 g/mL

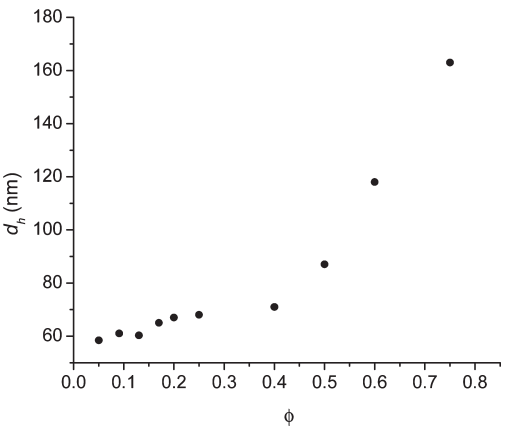

Figure 7. The dependence of the diameter of the clusters on the volume fraction of the droplet to continuous phase (C = 50 mM and f = 0.05 g/mL).

and 0.4 g/mL were found to be weakly shear thickening with viscosities of 1.7 cP and 2.6 cP at shear rates of 250 s^{-1}, respectively, whereas 50 mM SDS solutions have a viscosity of 2.4 cP at a shear rate of 250 s^{-1}(Supporting Information). Hence, λ is near unity for f = 0.4 g/mL and decreases as f decreases (we estimate that, for f = 0.025 g/mL, the viscosity of the droplet phase approaches that of pure toluene, 0.59 cP). It has been shown that the viscous shear force required to break up a droplet is near a minimum when $\lambda \sim 1$ and increases for decreasing λ.[42] On the basis of this finding, we hypothesize that the droplet size decreases with increasing concentration of SPM NPs as a result of λ approaching a value of unity. Therefore, the concentration of the SPM NPs in the droplet phase influences the cluster sizes not only by establishing the number of SPM NPs per droplet, but also by governing the size of the droplet formed during shearing.

The dependence of the cluster size on the volume fraction of the droplet phase, ϕ, was examined for ratios ranging from 0.05 to 0.75. The diameter of the clusters formed under these conditions, shown in Figure 7, shows two distinct size dependencies reflecting two distinct emulsification behaviors. Below $\phi \sim 0.4$, the size of the clusters (or droplets) shows a weak dependence on volume fraction of the droplet phase, whereas above $\phi \sim 0.5$, the size of the clusters (or droplets) increases dramatically with the volume fraction of the droplet phase. The transition between the two regimes coincides with the concentration at which emulsion droplets begin to pack. It has been shown elsewhere that, as droplets begin to pack in highly concentrated emulsions, the emulsions exhibit larger elastic shear modulus and, as a result, undergo significant changes in their flow properties.[35,43] To confirm this effect, we measured the viscosity of an emulsion made from two volume fractions of the droplet phase (ϕ = 0.09 and 0.5 with C = 50 mM and f = 0.05 g/mL) (see Supporting Information). The emulsions prepared at ϕ = 0.09 revealed shear thinning behavior with viscosities leveling at 2 cP at high shear rates. This value of viscosity is commensurate with the viscosity of the SDS solutions, demonstrating that, at this volume fraction, the emulsion viscosity is governed by the viscosity of the continuous phase. The emulsion prepared at ϕ = 0.5 also displayed shear thinning behavior, but, in contrast to the emulsion prepared at low droplet phase fraction, the viscosity of this emulsion leveled at 15 cP at high shear rates. This relatively high value of viscosity demonstrates

(42) Liu, X. Q.; Guan, Y. P.; Ma, Z. Y.; Liu, H. Z. *Langmuir* **2004**, *20*, 10278–10282.
(43) Saiki, Y.; Horn, R. G.; Prestidge, C. A. *J. Colloid Interface Sci.* **2008**, *320*, 569–574.

that the flow properties are governed by the emulsion as a whole. In this regime of high packing density of emulsion droplets, it has been shown that fractured flow occurs between planes of droplets, causing droplets to slip by each other without elongating and rupturing the droplets.[35,36] Therefore, larger droplets (and clusters) form as the volume fraction of the droplet phase increases.

3.2.4. Polydispersity. Controlling the size dispersion of the clusters is important, as it sets the size distribution of the nanobeads as a whole. On the basis of TEM image analysis, the clusters generally had size distributions with coefficients of variation of approximately 25%. We observed that the size distribution was partly governed by the method used to shear. For instance, we found that emulsifying with a shear dispersant (IKA Ultra-Turrax) generated clusters with a broader size distribution than those generated by ultrasonicating. In addition, certain emulsion compositions appeared to broaden the size distribution. More specifically, small clusters containing only a few nanoparticles formed under particular conditions. This was observed on TEM images as a background of undefined aggregates of SPM NPs, as shown in Figure 8a,b. Conditions that tended to promote their formation included emulsions with low surfactant concentration (< 10 mM), as shown in Figure 8a. We believe that, under low surfactant concentrations, droplets can have a heterogeneous distribution of surfactant on their surface, where, during emulsification, the surfactant preferentially collects at the tip of the elongated droplet, causing the ends to pinch off as small droplets.[38,44] Similar undefined aggregates of SPM NPs were observed when low concentrations of SPM NPs were used, as shown in Figure 8b. The low droplet viscosity could likewise contribute to the formation of small satellite droplets during droplet rupturing. As shown in Figure 8c,d, well-defined clusters with narrower size distributions were obtained for high concentrations of SPM NPs or high fractions of the droplet with respect to the continuous phase. As has been shown elsewhere, we are currently exploring whether continuous phases with higher viscosities can lead to further decreases in the size distribution by minimizing the fracturing of flow.[34] We note that since magnetic clusters have magnetophoretic mobilities that vary as $\sim r^2$, the size distribution of clusters can be narrowed using an applied magnetic field.[4] That is, dispersions of clusters can be size fractionated by collecting clusters of a specific size based on their magnetic confinement rate.

To summarize, clusters of SPM NPs were prepared by emulsifying SPM NPs, dispersed in toluene, into aqueous solutions of surfactant and condensing the droplets. Several key features of the process of forming clusters can be made:

1 Once the droplets are formed, droplets do not coalesce, and SPM NPs do not diffuse from droplet to droplet. Therefore, the size and size distribution of the clusters are defined by the droplets made during emulsification and, as a result, are determined by the emulsification conditions and emulsion composition.
2 Parameters such as the concentration of the surfactant, the volume fraction of the droplet phase, and the concentration of the SPM NPs influence the viscosity ratio of the droplet to continuous phase, the degree of fractured flow, and the interfacial tension and, as a result, govern the size of the clusters. The size of the clusters is most conveniently controlled by varying the concentration of SPM NPs in the droplet phase.
3 The size distribution can be narrowed by using high volume fraction of droplet phase.

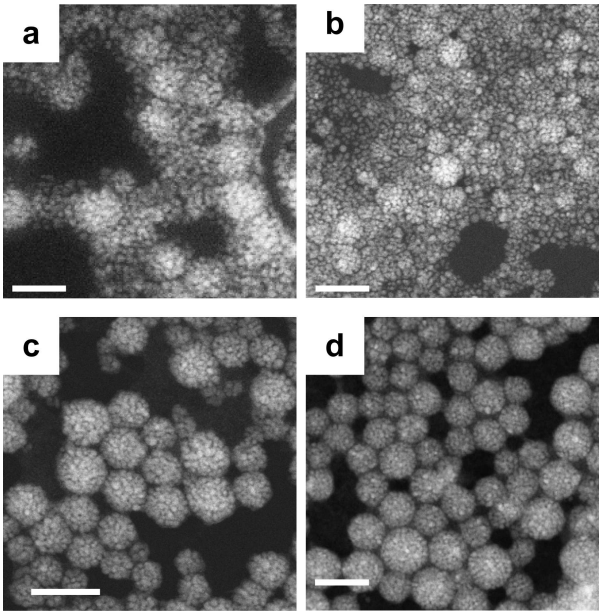

Figure 8. TEM images of clusters prepared with (a) low concentration of SDS (C = 3 mM, f = 0.05 g/mL, $\phi = 0.09$), (b) low concentration of SPM NPs (f = 0.05 g/mL, ϕ = 0.09, C = 50 mM), (c) high concentration of SPM NPs (f = 0.2 g/mL, ϕ = 0.09, C = 50 mM), and (d) high volume fraction of the droplet phase (f = 0.05 g/mL, ϕ = 0.65, C = 50 mM). Scale bar: 100 nm.

3.3. Preparation and Characterization of the Nanobeads. Clusters of nanoparticles were encapsulated in a polymer shell by inducing polymerization at the interface of the clusters, forming functional superparamagnetic nanobeads. By introducing a monomer, such as methyl methacrylate, styrene, and/or acrylic acid, seconds before thermo-initiation, it was possible to avoid significant swelling of clusters by the monomer bringing about polymerization at the interface of the clusters. This scenario is similar to a seeded-emulsion polymerization, although here the clusters act as seeds.[45,46] We note, however, that when the concentration of SDS was above the critical micelle concentration, colloids with no magnetic core (i.e., polymer colloids) formed along with clusters coated with a polymer shell. This result indicates that secondary nucleation of polymer particles can occur in micelles, thereby diverting monomer to forming these particles instead of coating the clusters. When the SDS concentration was below the critical micelle concentration, only polymer-coated clusters were observed. Therefore, to achieve polymerization at the interface of the clusters and prevent nucleation and polymerization in micelles, the concentration of the SDS in the dispersion of clusters must be below the critical micelle concentration of SDS, but high enough to maintain stability of the clusters (i.e., 1−5 mM SDS).

The shells, shown in Figure 1b,c and Figure 9a, have two important functions. First, the polymer shells render the clusters more robust. For instance, when HCl is mixed with the polymer-coated clusters, the clusters retained their magnetic properties,

(44) Groeneweg, F.; van Dieren, F.; Agterof, W. G. M. *Colloids Surf. A* **1994**, *91*, 207–214.

(45) Wang, Z.; Paine, A. J.; Rudin, A. *J. Colloid Interface Sci.* **1996**, *177*, 602–612.

(46) Wang, D.; Dimonie, V. L.; Sudol, D. E.; El-Aasser, M. S. *J. Appl. Polym. Sci.* **2002**, *84*, 2710–2720.

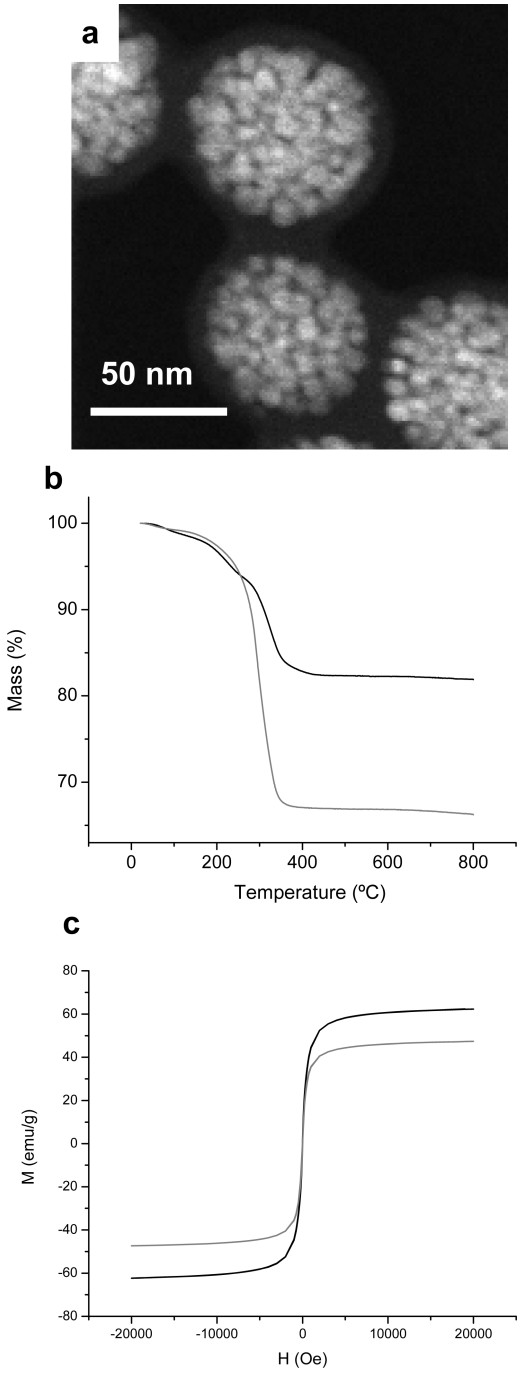

Figure 9. (a) TEM image of nanobeads formed from encapsulating clusters of SPM NPs (d = 71 nm) with a polymer shell (d = 8 nm). (b) TGA of the clusters (black curve) and the nanobeads (gray curve). (c) Mass magnetization curves at 300 K of clusters (black curve) and the nanobeads (gray curve).

indicating that HCl cannot diffuse across the polymer layer to dissolve the iron oxide NPs. Second, functionality can be incorporated into the polymer shells by copolymerizing with a functional monomer, such as acrylic acid or GMA. It should also be noted that an important advantage of this polymerization mechanisms is that the thickness of the shell can easily be adjust by simply varying the amount of monomer. This feature is important particularly when only a thin shell is desired to maintain the high loading of SPM NPs.

To demonstrate key properties of nanobeads prepared through this approach, we prepared clusters of 71 ± 8 nm and polymerized a shell of 8 ± 1 nm by copolymerizing GMA and EGDMA. The nanobeads are shown in Figure 9a. In order to demonstrate the high density of functional groups provided by this method, Lucifer yellow cadavarine was reacted with the nanobeads post polymerization. On the basis of the photoluminescence of purified beads, the nanobeads possessed a density of 1.5 dye molecules/nm^2. Therefore, this approach can provide a high density of functional groups required for attaching molecular recognition agents to the surface of the nanobeads.

The high content of SPM NPs of the clusters and nanobeads was revealed by TGA analysis. The clusters showed a mass loss of 17%, indicating that the clusters are made up of 83% of the magnetic component, iron oxide. This value is commensurate with the mass loss of individual SPM NPs. The mass loss thus originates from the organic ligands stabilizing the SPM NPs. Figure 9b shows that, by adding a shell of 8 nm, the magnetic component of the nanobeads is 66% wt. Although it is possible to form thinner shells and increase the fraction of magnetic material, these nanobeads have nonetheless a high concentration of iron oxide nanoparticles, imparting them with high saturation magnetization. As shown in Figure 9c, the saturation magnetization of the cluster is 62 emu/g, which is similar to that of individual SPM NPs (see Supporting Information), while for the nanobeads with an 8 nm shell, it is 47 emu/g at 300 K. This value of saturation magnetization for the nanobeads is comparatively high. Reported values of saturation magnetization for superparamagnetic colloids typically lie in the range of 4−30 emu/g with the exception of a Xu and coworkers report describing colloids with 40 emu/g and Ge and co-workers describing their aggregates as possessing a saturation magnetization of 63 emu/g.[21,24,42,47−49] The magnetization curves of the clusters and the nanobeads show zero coercivity, indicating that the clusters and the nanobeads preserve their superparamagnetic behavior.

In summary, the encapsulation of the clusters to generate nanobeads renders the clusters functional by increasing their robustness and providing a high density of functional surface groups. Since the thickness of the polymer shell can be controlled, this approach offers a means to minimize the amount of nonmagnetic material and maintain a high saturation magnetization. Because of their high saturation magnetization, these nanobeads are expected to respond rapidly to applied magnetic field gradients despite their small size.

4. Conclusion

A route to preparing superparamagnetic nanobeads was developed using emulsification and seeded-emulsion polymerization concepts. The structure of the colloids is designed to minimize the amount of nonmagnetic material while maximizing the amount of SPM NPs. The beads consist of a core of densely packed SPM NPs encapsulated in a thin polymer shell. The thin polymer shell provides a high density of functional groups for postsynthesis surface modifications. The approach is ideal for generating hybrid colloids with superparamagnetic functionality, as they possess a high loading of nanoparticles and, as a result, possess high saturation magnetizations. These properties make them ideal structures for use in biomedical application such as substrates, probes, and drug delivery vehicles.

(47) Xia, A.; Hu, J. H.; Wang, C. C.; Jiang, D. L. *Small* **2007**, *3*, 1811–1817.
(48) Xu, X.; Friedman, G.; Humfeld, K. D.; Majetich, S. A.; Asher, S. A. *Chem. Mater.* **2002**, *14*, 1249–1256.
(49) Stjerndahl, M.; Andersson, M.; Hall, H. E.; Pajerowski, D. M.; Meisel, M. W.; Duran, R. S. *Langmuir* **2008**, *24*, 3532–3536.

Acknowledgment. We thank Professor Muralee Murugesu of the University of Ottawa for acquiring the magnetization curves, Michael Barnes for TGA analysis, and Ilya Gourevich from the Univeristy of Toronto for acquiring TEM images.

Supporting Information Available: Magnetization curves, viscosity measurements, and conductivity curves of SDS solutions. This material is available free of charge via the Internet at http://pubs.acs.org.